Pulmonary Lymphangitic Carcinomatosis: Diagnostic Performance of High-Resolution CT and ^{18}F-FDG PET/CT in Correlation with Clinical Pathologic Outcome

Mario Jreige*[1], Vincent Dunet*[2], Igor Letovanec[3], John O. Prior[1], Reto A. Meuli[2], Catherine Beigelman-Aubry[2], and Niklaus Schaefer[1]

[1]Department of Nuclear Medicine and Molecular Imaging, Lausanne University Hospital, Lausanne, Switzerland; [2]Department of Diagnostic and Interventional Radiology, Lausanne University Hospital, Lausanne, Switzerland; and [3]Institute of Pathology, Lausanne University Hospital, Lausanne, Switzerland

The rationale of this study was to investigate the performance of high-resolution CT (HRCT) versus ^{18}F-FDG PET/CT for the diagnosis of pulmonary lymphangitic carcinomatosis (PLC). **Methods:** In this retrospective institution-approved study, 94 patients addressed for initial staging of lung cancer with suspicion of PLC were included. Using double-blind analysis, we assessed the presence of signs favoring PLC on HRCT (smooth or nodular septal lines, subpleural nodularity, peribronchovascular thickening, satellite nodules, lymph node enlargement, and pleural effusion). ^{18}F-FDG PET/CT images were reviewed to qualitatively evaluate peritumoral uptake and to quantify tracer uptake in the tumoral and peritumoral areas. Histology performed on surgical specimens served as the gold standard for all patients. **Results:** Among 94 included patients, 73% (69/94) had histologically confirmed PLC. Peribronchovascular thickening, lymph node involvement, and increased peritumoral uptake were more often present in patients with PLC ($P < 0.009$). Metabolic variables, including tumor SUV_{max}, SUV_{mean}, metabolic tumor volume, and total lesion glycolysis, as well as peritumoral SUV_{max}, SUV_{mean}, and their respective ratios to background, were significantly higher in the PLC group than in the non-PLC group ($P \leq 0.0039$). Sensitivity, specificity, and area under the receiver-operating-characteristic curve for peribronchovascular thickening (69%, 83%, and 0.76, respectively; 95% confidence interval [95%CI], 0.67–0.85) and increased peritumoral uptake (94%, 84%, and 0.89, respectively; 95%CI, 0.81–0.97) were similar ($P = 0.054$). For detecting PLC, sensitivity, specificity, and area under the receiver-operating-characteristic curve were significantly higher, at 97%, 92%, and 0.98, respectively (95%CI, 0.96–1.00), for peritumoral SUV_{max} and 94%, 88%, and 0.96, respectively (95%CI, 0.92–1.00), for peritumoral SUV_{mean} (all $P \leq 0.025$). **Conclusion:** Qualitative evaluation of ^{18}F-FDG PET/CT and HRCT perform similarly for the diagnosis of PLC, with both being outperformed by ^{18}F-FDG PET/CT quantitative parameters.

Key Words: pulmonary lymphangitic carcinomatosis; lung cancer; PET/CT; FDG; HRCT

J Nucl Med 2020; 61:26–32
DOI: 10.2967/jnumed.119.229575

Received Apr. 9, 2019; revision accepted Jun. 5, 2019.
For correspondence or reprints contact: Catherine Beigelman-Aubry, Department of Diagnostic and Interventional Radiology, Lausanne University Hospital, Rue du Bugnon 46, CH-1011 Lausanne, Switzerland.
E-mail: catherine.beigelman-aubry@chuv.ch
*Contributed equally to this work.
Published online Jun. 21, 2019.

Pulmonary lymphangitic carcinomatosis (PLC) was first described by Troisier in 1873 and is morphologically defined by the presence of malignant cells within pulmonary vessels, in particular the lymphatics (*1*). Mainly originating from adenocarcinoma of the breast, stomach, lung, pancreas, and prostate, PLC may appear as a bilateral symmetric pattern in cases of hematogenous spread through the pulmonary arteries and subsequently into the perivascular interstitium and lymphatic vessels or as an asymmetric localized pattern with direct extension from primary lung tumor, hilar lymph nodes, or pleura (*2*). Even though a definitive diagnosis of PLC requires lung biopsy, high-resolution CT (HRCT) is considered an essential tool in the diagnostic process and is recommended before pathologic examination (*3–5*). The few studies that have investigated the role of ^{18}F-FDG PET or PET/CT in the diagnosis of PLC suggest that PET/CT has an effective and reliable role as a noninvasive technique allowing identification of PLC with high specificity (*6–8*). Regarding the diagnostic performance of ^{18}F-FDG PET/CT, data still remain spare compared with HRCT, and no study has formally evaluated the diagnostic value of quantitative PET/CT metrics compared with HRCT and PET/CT qualitative evaluations. We hence hypothesized that measurement of ^{18}F-FDG uptake in the peritumoral lung may help to detect PLC in patients with primary lung cancer.

The aim of this study was to investigate the performance of HRCT versus ^{18}F-FDG PET/CT for the diagnosis of PLC secondary to lung cancer, against the histologic gold standard, and to evaluate the added value of quantitative ^{18}F-FDG PET/CT metrics.

MATERIALS AND METHODS

Study Design

The study was conducted according to the 2015 Standards for Reporting of Diagnostic Accuracy Studies (*9*). All patients referred to our Institutional Thoracic Cancer Board from December 2012 to May 2016 after initial staging of untreated lung cancer were retrospectively reviewed. To be included, a patient had to have had both HRCT and ^{18}F-FDG PET/CT within 10 wk of each other for initial staging and had to have had surgical resection (i.e., segmentectomy, lobectomy, or pneumectomy) without neoadjuvant chemotherapy. Patients were excluded if there had been more than 10 wk between HRCT and ^{18}F-FDG PET/CT, if the ^{18}F-FDG PET/CT had been performed at a different institution, or if neoadjuvant chemotherapy had been given (Fig. 1). PLC, as defined by the presence of secondary invasive cells within the vessels in the peritumoral area, was ascertained on pathology

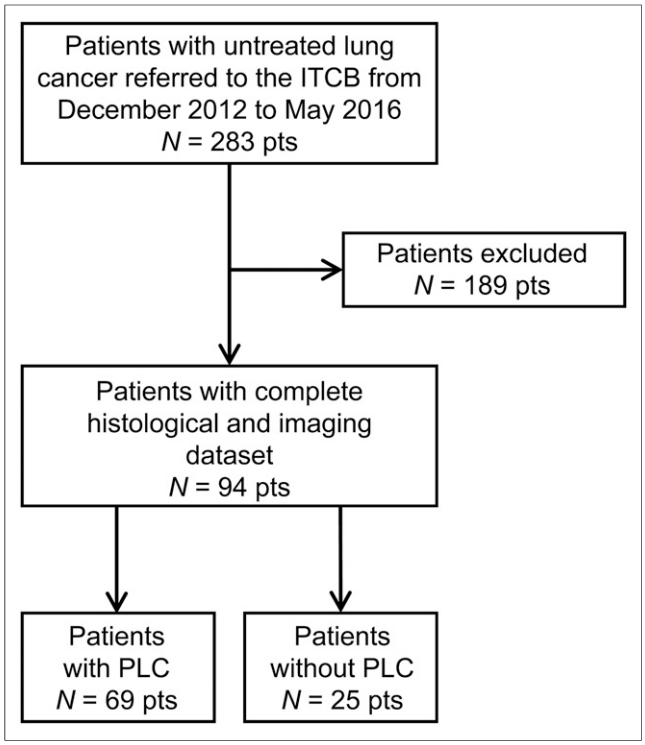

FIGURE 1. Study flowchart. ITCB = Institutional Thoracic Cancer Board.

reports, which were used as our gold standard. For all included patients, the presence of imaging signs of PLC was evaluated on HRCT and ^{18}F-FDG PET/CT based on a double-blind study and correlated with clinical pathology. The median delay between the 2 modalities was 3.5 wk (range, 0.1–10 wk). The local Ethics Research Committee of the State of Vaud approved the research protocol (CER-VD 2016-01295) and, because the study was retrospective, waived the need for informed consent.

^{18}F-FDG PET/CT Acquisition and Analysis

Patients underwent ^{18}F-FDG PET/CT on a Discovery D690 TOF (GE Healthcare) 50–70 min after a 3.7 ± 0.5 MBq/kg intravenous injection of ^{18}F-FDG. All patients fasted for at least 6 h and had blood glucose levels lower than 140 mg/dL before administration of ^{18}F-FDG. A low-dose helical CT scan was first performed for anatomic correlation and attenuation correction (tube voltage, 120–140 kV; tube current, 80–200 mA or mA automodulation; pitch, 1.375; time per rotation, 0.8 s; slice thickness, 3.75 mm). Raw data were reconstructed using a blend of 40% adaptive statistical iterative reconstruction and 60% filtered backprojection. Whole-body emission images were then acquired using 7–9 overlapping bed positions of 2 min each (starting from the top of the skull and ending at the mid thigh). Images were reconstructed using ordered-subset expectation maximization (8 subsets, 2 iterations) with body weight–normalized SUV computation.

For each patient, the SUV_{max} (g/mL), SUV_{mean} (g/mL), metabolic tumoral volume (cm^3), and total lesion glycolysis ($g \cdot cm^3$/mL) of the primary lung tumor were measured using a standard 42% SUV_{max} threshold volume of interest embedding the whole tumor. In addition, perilesional tumoral activity was visually compared with contralateral normal lung (0, not increased; 1, increased) and quantified by measurement of SUV_{max} and SUV_{mean} within a 3-cm peritumoral range using a 3 cm^3 volume of interest on the most active region. Normal lung background uptake, as defined by SUV_{mean} measured in a 3 cm^3 volume of interest within the contralateral normal lung, was used to calculate peritumoral uptake ratios as follows: peritumoral SUV_{max} ratio = peritumoral SUV_{max}/contralateral normal-lung SUV_{mean}. Peritumoral SUV_{max} and SUV_{mean} were measured twice by 2 nuclear physicians with 4 and 10 y of experience, masked to the histologic results, to assess interobserver reproducibility.

HRCT Acquisition and Analysis

Thoracic HRCT was performed on multidetector CT scanners from multiple vendors. Because the study was retrospective, the dose parameters varied due to the different acquisition protocols used (tube voltage, 80–120 kV; tube intensity, 80–400 mA or mA automodulation). All raw data were reconstructed by filtered backprojection using a soft lung kernel with 1-mm slice thickness.

HRCT images of the 94 included patients were analyzed in consensus by 2 radiologists with 25 and 10 y of experience in thoracic imaging, with masking of the histologic results. The presence of smooth lines, nodular septal lines, subpleural nodularity, peribronchovascular thickening, satellite nodules, lymph node enlargement, pleural effusion, and enlarged pulmonary veins adjacent to the primary lung tumor was recorded at the patient level (0, absent; 1, present).

Histologic Analysis

All surgical specimens were retrospectively collected and prospectively analyzed by a pathologist with more than 15 y of experience in thoracic pathology. The pathologist was masked to the imaging results at the time of histologic analysis. Resected lung specimens were fixed in formalin for 24–48 h. Representative samples of the tumor were taken, embedded in paraffin, sectioned onto slides, and stained with hematoxylin and eosin. PLC was defined as the presence of secondary invasive cells within vessels in the peritumoral area. Tumor typing was performed according to the 2011 International Association for the Study of Lung Cancer/2015 World Health Organization classification (*10*).

Statistical Analysis

All statistical analyses were performed using STATA, version 15.1 (STATA Corp.). Sample size was calculated to test the equality of HRCT and ^{18}F-FDG PET/CT. On the basis of a previous study by Prakash et al., we considered the accuracy of ^{18}F-FDG PET/CT to be 93% and the difference between the 2 methods to be 10% (*6*). Using a 2-sided McNemar test at an α level of 0.05, we determined that a sample size of 93 patients would achieve 80% power. Continuous variables are presented as mean ± SD or as median and interquartile range (IQR). Categoric variables are presented as number or percentage. Histologic outcome was used as the gold standard for the diagnosis of PLC. All collected variables derived from the analysis of HRCT and ^{18}F-FDG PET/CT were then compared between patients with and without PLC using the Kruskal–Wallis test for continuous variables and the Fisher exact test for categoric variables. The interobserver reproducibility of peritumoral SUV_{max} and SUV_{mean} was assessed by the Pearson correlation coefficient (ρ) and the Lin concordance correlation coefficient ($\rho_c = \rho \times C_b$, with C_b being a measurement of systematic bias) (*11*). The association between imaging variables and PLC was assessed using logistic regression analysis with computation of respective odds ratios (ORs) and 95% confidence intervals (95%CIs). The ORs of significant predictors were compared using the Hausman specification test. Receiver-operating-characteristic (ROC) curves were also analyzed, with computation of area under the ROC curve (ROC area), sensitivity, specificity, positive and negative likelihood ratios, and respective 95%CI for each variable. For continuous variables, optimal cutoffs allowing detection of patients with PLC were determined by the Liu method (*12*).

ROC areas were compared for HRCT and ^{18}F-FDG PET/CT variables that were significantly associated with PLC on univariate logistic regression analysis (i.e., peribronchovascular thickening, increased peritumoral uptake, and peritumoral SUV_{max} and SUV_{mean}) using the nonparametric χ^2 test of equality for ROC areas, as defined by DeLong et al. (*13*). For this comparison, we used multiple imaging parameters on univariate analysis, and the significance level was corrected by the Bonferroni method to account for multiple testing. *P* values of less than 0.003 were considered statistically significant.

RESULTS

Study Population

Overall, 94 patients (67 men and 27 women; median age, 68 y; range, 44–87 y) were retrospectively included (Table 1). All underwent surgical resection and histologic analysis of surgical specimens a mean of 5.9 wk (range, 0.6–22.8 mo) after the initial imaging evaluation. Of the 94 patients, 29 had stage 1 disease, 29 had stage 2 disease, 34 had stage 3 disease, and 2 had stage 4 disease according to the eighth edition of the TNM classification

TABLE 1
Clinicopathologic Characteristics and Results of HRCT and ^{18}F-FDG PET/CT Evaluation in Patients Without and With PLC

Variable	Without PLC, *n* = 25	With PLC, *n* = 69	*P*
Age (y)	67 ± 10	66 ± 9	0.81
Sex (M/F)	18/7	49/20	0.57
TNM stage			<0.001
1	16	13	
2	6	23	
3	2	32	
4	1	1	
Surgery			0.21
Segmentectomy	3	4	
Lobectomy	22	59	
Pneumonectomy	0	6	
Histology			0.081
Adenocarcinoma	19	36	
Poorly differentiated NSCLC	0	5	
Squamous cell carcinoma	6	28	
HRCT			
Smooth lines	19	60	0.45
Nodular lines	3	13	0.62
Peribronchovascular thickening	4	46	0.0002
Subpleural space	3	4	0.64
Satellite nodes	6	12	0.61
Enlarged lymph nodes	7	44	0.0082
Pleural effusion	3	9	0.95
Enlarged pulmonary veins	4	4	0.44
PET qualitative (peritumoral increased uptake)	4	65	0.0001
PET quantitative			
Tumor SUV_{max} (g/mL)	9.1 ± 7.1	14.1 ± 8.0	0.0031
Tumor SUV_{mean} (g/mL)	5.5 ± 4.7	8.4 ± 5.1	0.0039
MTV (cm^3)	9.6 ± 9.4	22.3 ± 23.3	0.0031
TLG ($g \cdot cm^3$/mL)	72.9 ± 119.4	225.8 ± 322.7	0.0006
Peritumoral SUV_{max} (g/mL)	1.5 ± 0.4	3.2 ± 0.6	0.0001
Peritumoral SUV_{mean} (g/mL)	0.9 ± 0.3	1.8 ± 0.4	0.0001
Peritumoral SUV_{max} ratio	1.6 ± 0.5	3.2 ± 0.7	0.0001
Peritumoral SUV_{mean} ratio	1.7 ± 0.6	3.1 ± 0.9	0.0001

NSCLC = non–small cell lung carcinoma; MTV = metabolic tumoral volume; TLG = total lesion glycolysis.

Qualitative data are expressed as numbers; continuous data are expressed as mean ± SD. *P* values were obtained using Kruskal–Wallis test for continuous variables and Fisher exact test for categoric variables. For imaging parameters, $P < 0.003$ was considered statistically significant to account for multiple comparisons.

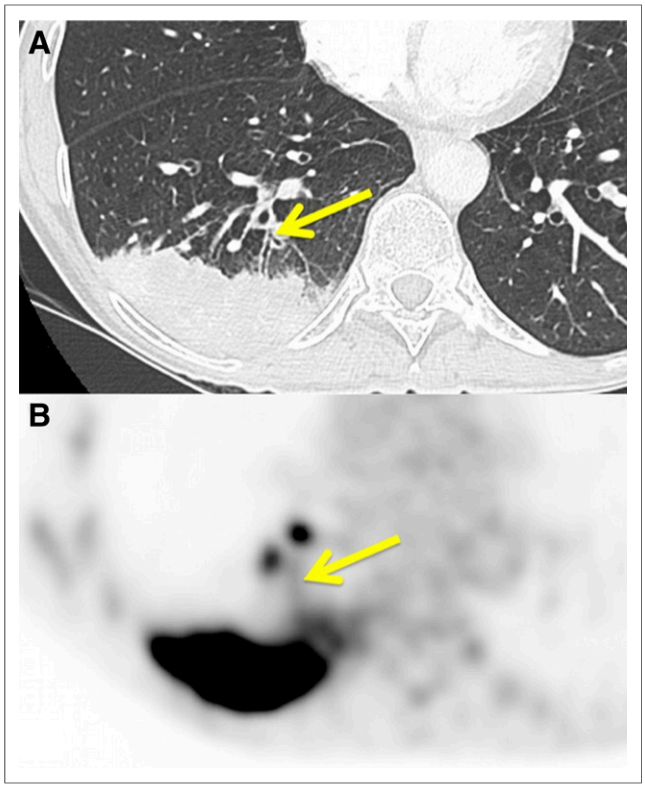

FIGURE 2. Case of 66-y-old woman referred for initial staging of inferior lobe pulmonary adenocarcinoma (stage IIIA, arrow). (A) HRCT shows positive peribronchovascular thickening sign. (B) ^{18}F-FDG PET/CT shows ^{18}F-FDG uptake higher than background in corresponding region, with SUV_{max} of 2.5 g/mL and SUV_{max}-to-background ratio of 3.6.

for lung cancer (*14*). Six patients underwent pneumonectomy, 81 patients lobectomy, and 7 patients segmentectomy. Fifty-five patients had adenocarcinoma, 34 patients squamous cell carcinoma, and 5 patients poorly differentiated non–small cell carcinoma. Histologic analysis additionally confirmed PLC in 69 of the 94 patients (73%).

Qualitative HRCT and ^{18}F-FDG PET/CT Analyses

All HRCT results are displayed in Table 1. There were no missing data for either imaging method. Only peribronchovascular thickening (Fig. 2) was significantly correlated with the presence of PLC (OR, 10.95; 95%CI, 3.33–36.0; $P < 0.001$; Table 2), showing an ROC area, sensitivity, specificity, and positive and negative likelihood ratios of 0.76 (95%CI, 0.67–0.85), 69%, 83%, 4.12, and 0.38, respectively. The presence of increased peritumoral uptake in comparison to lung background performed similarly to peribronchovascular thickening, with an ROC area, sensitivity, and specificity of 0.89 (95%CI, 0.81–0.97), 94%, and 84%, respectively ($P = 0.054$; Table 3).

Quantitative ^{18}F-FDG PET/CT Analysis

The interobserver reproducibility of peritumoral SUV_{max} measurement ($\rho = 0.922$, $\rho_c = 0.921$, $C_b = 1.0$) and SUV_{mean} measurement ($\rho = 0.850$, $\rho_c = 0.850$, $C_b = 1.0$) was excellent. Metabolic variables, including tumor total lesion glycolysis, peritumoral SUV_{max}, peritumoral SUV_{mean}, and their respective ratios to background, were significantly higher in patients with PLC than in patients without PLC ($P = 0.0006$, 0.0001, 0.0001, 0.0001, and 0.0001, respectively; Table 1). Peritumoral SUV_{max} and SUV_{mean},

TABLE 2
Results of Association of HRCT Variables with PLC

Variable	OR	*P*	ROC area	Se	Sp	LR+	LR−
Smooth lines	2.26 (0.64–7.94)	0.21	0.55 (0.46–0.64)	0.90 (0.80–0.96)	0.21 (0.07–0.42)	1.13 (0.91–1.41)	0.50 (0.18–1.43)
Nodular lines	1.69 (0.44–6.52)	0.45	0.53 (0.45–0.62)	0.19 (0.11–0.31)	0.88 (0.68–0.97)	1.55 (0.48–4.98)	0.92 (0.76–1.12)
Peribronchovascular thickening	10.95 (3.33–36.0)	<0.001	0.76 (0.67–0.85)	0.69 (0.56–0.79)	0.83 (0.63–0.95)	4.12 (1.66–10.2)	0.38 (0.25–0.56)
Subpleural space	0.44 (0.09–2.15)	0.31	0.47 (0.39–0.54)	0.06 (0.02–0.15)	0.88 (0.68–0.97)	0.48 (0.12–1.98)	1.07 (0.91–1.26)
Satellite nodes	0.65 (0.21–2.00)	0.46	0.46 (0.36–0.56)	0.18 (0.10–0.29)	0.75 (0.53–0.90)	0.72 (0.30–1.70)	1.09 (0.85–1.41)
Enlarged lymph nodes	4.65 (1.68–12.8)	0.003	0.68 (0.57–0.79)	0.66 (0.53–0.77)	0.71 (0.49–0.87)	2.25 (1.18–4.3)	0.48 (0.32–0.74)
Pleural effusion	1.09 (0.27–4.40)	0.91	0.50 (0.43–0.58)	0.13 (0.06–0.24)	0.88 (0.68–0.97)	1.07 (0.32–3.64)	0.99 (0.83–1.18)
Enlarged pulmonary veins	0.32 (0.07–1.39)	0.13	0.45 (0.37–0.53)	0.06 (0.02–0.15)	0.83 (0.63–0.95)	0.36 (0.10–1.32)	1.13 (0.93–1.36)

Se = sensitivity; Sp = specificity; LR+ = positive likelihood ratio; LR− = negative likelihood ratio.
Data in parentheses are 95%CI. $P < 0.003$ was considered statistically significant to account for multiple testing.

TABLE 3
Results of Association of ^{18}F-FDG PET/CT Variables with PLC

Variable	OR	*P*	ROC area	Cutoff	Se	Sp	LR+	LR−
PET qualitative (peritumoral increased uptake)	85.31 (19.6–371)	<0.001	0.89 (0.81–0.97)	—	0.94 (0.86–0.98)	0.84 (0.64–0.96)	5.89 (2.39–14.5)	0.07 (0.03–0.18)
PET quantitative								
Tumor SUV_{max} (g/mL)	1.10 (1.02–1.18)	0.011	0.70 (0.58–0.83)	9.1	0.74 (0.62–0.84)	0.64 (0.43–0.82)	2.05 (1.2–3.53)	0.41 (0.25–0.67)
Tumor SUV_{mean} (g/mL)	1.15 (1.02–1.29)	0.019	0.70 (0.57–0.82)	5.5	0.73 (0.60–0.83)	0.64 (0.43–0.82)	2.01 (1.17–3.46)	0.43 (0.27–0.70)
MTV (cm^3)	1.06 (1.00–1.11)	0.022	0.70 (0.58–0.82)	11.3	0.55 (0.43–0.67)	0.76 (0.55–0.91)	2.29 (1.11–4.76)	0.59 (0.42–0.83)
TLG ($g{\cdot}cm^3$/mL)	1.00 (1.00–1.01)	0.027	0.73 (0.61–0.85)	14.6	0.90 (0.80–0.96)	0.52 (0.31–0.72)	1.87 (1.24–2.84)	0.20 (0.09–0.43)
Peritumoral SUV_{max} (g/mL)	312 (13.7–7124)	<0.001	0.98 (0.96–1.00)	2.1	0.97 (0.90–1.00)	0.92 (0.74–0.99)	12.14 (3.21–45.9)	0.03 (0.01–0.12)
Peritumoral SUV_{mean} (g/mL)	724 (41.70–12,593)	<0.001	0.96 (0.92–1.00)	1.2	0.94 (0.86–0.98)	0.88 (0.69–0.98)	7.85 (2.71–22.7)	0.07 (0.03–0.17)
Peritumoral SUV_{max} ratio	63.0 (9.89–401)	<0.001	0.96 (0.92–1.00)	2.3	0.93 (0.84–0.98)	0.88 (0.69–0.98)	7.73 (2.67–22.4)	0.08 (0.04–0.19)
Peritumoral SUV_{mean} ratio	16.9 (5.24–54.5)	<0.001	0.92 (0.84–0.99)	2.4	0.84 (0.73–0.92)	0.92 (0.74–0.99)	10.51 (2.77–39.9)	0.17 (0.10–0.30)

Se = sensitivity; Sp = specificity; LR+ = positive likelihood ratio; LR− = negative likelihood ratio; MTV = metabolic tumor volume, TLG = total lesion glycolysis.
Data in parentheses are 95%CI. $P < 0.003$ was considered statistically significant to account for multiple testing. Cutoffs were determined by Liu method.

but not tumoral quantitative parameters, were highly associated with PLC (Fig. 3; Table 3). Peritumoral SUV_{max} and SUV_{mean} ORs were significantly higher than the ORs for qualitatively increased peritumoral uptake ($P = 0.0022$ and 0.0005, respectively) and than the ORs for peribronchovascular thickening ($P = 0.0004$ and $P < 0.0001$, respectively). Peritumoral SUV_{max} with a cutoff of 2.1 g/mL had a significantly higher sensitivity, specificity, and ROC area of 97%, 92%, and 0.98 (95%CI, 0.96–1.00), respectively, for detecting PLC than did either qualitatively increased peritumoral uptake ($P = 0.0064$) or peribronchovascular thickening ($P < 0.0001$; Fig. 4). Peritumoral SUV_{mean} with a cutoff of 1.2 g/mL also had higher performance for detecting PLC than did increased peritumoral uptake ($P = 0.025$) or peribronchovascular thickening ($P < 0.0001$). The diagnostic performance of absolute peritumoral SUV_{max}, peritumoral SUV_{mean}, peritumoral SUV_{max} ratio, and peritumoral SUV_{mean} ratio was similar ($P \geq 0.10$).

DISCUSSION

In this study, we showed that ^{18}F-FDG PET/CT and HRCT performed similarly in the diagnosis of PLC in patients addressed for initial staging of primary lung tumor when qualitatively evaluating, respectively, increased peritumoral uptake and peribronchovascular thickening. Other signs, such as smooth or nodular septal lines, subpleural nodularity, satellite nodules, and pleural effusion, were not significantly associated with PLC. Moreover, quantification of ^{18}F-FDG uptake in the peritumoral area outperformed qualitative analysis of either modality.

The pathogenesis of pulmonary tumor embolism and lymphangitic carcinomatosis is poorly understood. It is thought that, in PLC, tumor cells gain access to the lung vascular system—and particularly to the lymphatic system—to induce local tumoral spread via the neovasculature or neolymphatics when the primary tumor is of the lung. When the primary tumor is nonpulmonary, the cells spread via retrograde flow since most of these malignancies involve the thoracic lymph nodes. Tumor cell invasion via the interstitial space or distended lymphatic vessels can result in thickened peribronchovascular bundles and septa (*15–17*). Tumor cells trapped within lymphatics result in local obstruction and fluid accumulation. Thus, peribronchovascular bundles and alveolar septal thickening

FIGURE 3. Box plot showing significant difference in SUV_{max} in peritumoral region on ^{18}F-FDG PET/CT in patients with PLC (PLC+) and without PLC (PLC–).

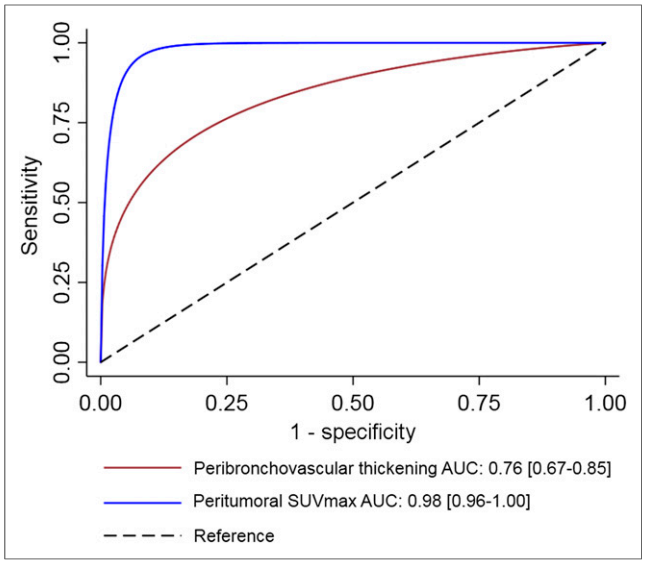

FIGURE 4. ROC curves comparing performance of peribronchovascular thickening on HRCT, and performance of SUV_{max} in peritumoral region on ^{18}F-FDG PET/CT, for diagnosis of PLC ($P < 0.0001$). Data in brackets are 95%CI.

may be due to local edema (*1*). Any malignant tumor has the potential to result in pulmonary tumor embolism, whether as PLC or as pulmonary tumor emboli, with a higher incidence in patients who have renal cell carcinoma, hepatocellular carcinoma, or adenocarcinoma of the breast, stomach, colon, or lung (*18,19*). This pattern of tumor spread is not common and occurs in less than 10% of metastatic cancers in the lung (*2*). The definitive diagnosis of PLC depends on the identification of tumor cells in the pulmonary lymphatics on histologic examination, which allows detection of obstruction and distension of pleural, peribronchial, perivascular, or subpleural lymphatics (*17*). PLC is typically an advanced-stage manifestation of malignancy and is associated with a poor prognosis (*20–22*).

Common findings associated with PLC on HRCT include thickening of interlobular septa and the peribronchovascular interstitium, subpleural nodules, thickening of the interlobar fissures, pleural effusion, pleural carcinomatosis, and hilar and mediastinal nodal enlargement, with relatively little destruction of overall lung architecture (*4*). However, smooth or thickened interlobular septa on HRCT, in particular with a nodular appearance, are not specific for PLC because these findings are also encountered in other interstitial disorders, such as sarcoidosis (*23*). Hilar adenopathy and effusions were occasionally present in reported series of PLC (*24*).

In a retrospective study on 21 patients, when correlated with pathology results, certain characteristic findings on CT scans were evident: uneven thickening of peribronchovascular bundles, thickening of isolated interstitial lines, and the presence of polygonal lines. The pathologic basis for these characteristic CT findings was considered by the authors as related to tumor thrombi in lymphatic vessels rather than to edema and fibrosis, at least in the early stages of disease (*25*). Another study reported that thickening of peribronchovascular bundles and interlobular septa is the single most important chest CT finding of PLC (*26*). Our study hereby confirms that peribronchovascular thickening and lymph node enlargement should be considered signs of PLC mainly at initial staging; it is the first report of diagnostic performance of HRCT in this setting to our knowledge.

Regarding ^{18}F-FDG PET/CT, to our knowledge we have described the largest series of patients who had histologically proven PLC and underwent imaging with a state-of-the art ^{18}F-FDG PET/CT scanner. To the best of our knowledge, only 3 studies have reported the role of ^{18}F-FDG PET/CT in the diagnosis of PLC. In a retrospective study of 35 patients, Prakash et al. found a high specificity of 100% for ^{18}F-FDG PET/CT in the detection of PLC, with a sensitivity of 86% (*6*). In addition, that study reported a statistically significant increased ^{18}F-FDG uptake in the PLC areas in contrast to normal lung parenchyma and blood-pool activity, in concordance with our results. In a group of 7 patients with PLC, Digumarthy et al. reported that the intensity of ^{18}F-FDG uptake was significantly greater in diseased lung than in corresponding normal contralateral lung or in the lungs of healthy controls, with the SUV ratio for diseased to normal tissue being significantly increased (*8*). In a series of 5 PLC-positive cases, Acikgoz et al. described the ^{18}F-FDG PET/CT pattern as varying from a diffuse, lobar, or segmental ^{18}F-FDG uptake in the lungs in extensive PLC to a hazy area of ^{18}F-FDG uptake or linear uptake extending from the tumor to the lymph nodes in limited PLC (*7*). The route of lymphangitic spread in these cases was considered to be either through seeding of tumor cells to the peribronchovascular lymphatics or through direct invasion of lymphatics by the lung tumor. Although we confirmed that increased peritumoral uptake may be useful in the detection of PLC, its performance was not superior to that of peribronchovascular thickening on HRCT. Moreover, we demonstrated that adding peritumoral SUV and ratio to lung background measurement significantly improved the performance of ^{18}F-FDG PET/CT for the diagnosis of PLC. Quantitative ^{18}F-FDG PET/CT of peritumoral areas should hence be part of the initial imaging workup of patients with primary lung cancer. However, CT images should always be checked before peritumoral SUV is measured, to avoid misinterpreting peritumoral infiltrates for another etiology, such as infection (*27*). In hybrid imaging, acquisition of HRCT images during a single contrast-enhanced ^{18}F-FDG PET/HRCT examination should be the next step to optimize patients' evaluation and minimize costs and needs to be investigated further.

We have to address some limitations of our study. First, because the study was retrospective, HRCT images were acquired on CT scanners from multiple vendors and with variable acquisition parameters but similar reconstruction parameters. Although image quality may differ, such variations reflect the daily practice of our Institutional Thoracic Cancer Board. Second, HRCT images were assessed by experts in thoracic imaging. Although qualitative evaluation of HRCT and ^{18}F-FDG PET/CT demonstrated similar performance, the learning curve to detect subtle peribronchovascular thickening on HRCT may be an issue in reproducing this result in daily practice, especially in situations such as COPD patients with bronchial wall thickening. Third, only patients who underwent surgical resection were included. Although this criterion allowed histologic confirmation of PLC, reported cutoffs for quantitative metrics may not be fully transposable to inoperable patients or to the use of different PET scanners or reconstruction algorithms. However, use of peritumoral SUV ratios may overwhelm this limitation, with similar diagnostic confidence. Finally, whereas the use of ^{18}F-FDG PET/CT quantitative parameters improved the diagnostic performance of ^{18}F-FDG PET/CT for PLC, the prognostic value of these metrics at initial staging remains unknown. This area of investigation was outside the scope of the present study and should be further assessed to fully evaluate the usefulness of these measurements.

CONCLUSION

Our study showed that peribronchovascular thickening and increased peritumoral tracer uptake on, respectively, HRCT and ^{18}F-FDG PET/CT performed similarly for the diagnosis of PLC in patients with lung cancer at initial staging. Peritumoral ^{18}F-FDG uptake quantification, however, outperformed qualitative evaluation. Combining the resultant morphologic and metabolic criteria may thus help to establish a powerful tool for the diagnosis of PLC.

DISCLOSURE

No potential conflict of interest relevant to this article was reported.

KEY POINTS

QUESTION: How do the performance of HRCT and ^{18}F-FDG PET/CT compare for the diagnosis of PLC?

PERTINENT FINDINGS: Peribronchovascular thickening and increased peritumoral tracer uptake on, respectively, HRCT and ^{18}F-FDG PET/CT perform similarly for the diagnosis of PLC in patients with lung cancer at initial staging. Peritumoral ^{18}F-FDG uptake quantification, however, outperforms qualitative evaluation on either modality.

IMPLICATIONS FOR PATIENT CARE: Combining morphologic and metabolic parameters may help establish a powerful tool for the diagnosis of PLC.

REFERENCES

1. Bruce DM, Heys SD, Eremin O. Lymphangitis carcinomatosa: a literature review. *J R Coll Surg Edinb.* 1996;41:7–13.
2. Janower ML, Blennerhassett JB. Lymphangitic spread of metastatic cancer to the lung: a radiologic-pathologic classification. *Radiology.* 1971;101:267–273.
3. Regueiro F, Roche P, Regueiro MV, Lozano R. The importance of histology in the evaluation of pulmonary transplantation: carcinomatous lymphangitis. *Thorac Cardiovasc Surg.* 2005;53:122–123.
4. Torrington KG, Hooper RG. Diagnosis of lymphangitic carcinomatosis by transbronchial lung biopsy. *South Med J.* 1978;71:1487–1488.
5. Mathieson JR, Mayo JR, Staples CA, Muller NL. Chronic diffuse infiltrative lung disease: comparison of diagnostic accuracy of CT and chest radiography. *Radiology.* 1989;171:111–116.
6. Prakash P, Kalra MK, Sharma A, Shepard JA, Digumarthy SR. FDG PET/CT in assessment of pulmonary lymphangitic carcinomatosis. *AJR.* 2010;194:231–236.
7. Acikgoz G, Kim SM, Houseni M, Cermik TF, Intenzo CM, Alavi A. Pulmonary lymphangitic carcinomatosis (PLC): spectrum of FDG-PET findings. *Clin Nucl Med.* 2006;31:673–678.
8. Digumarthy SR, Fischman AJ, Kwek BH, Aquino SL. Fluorodeoxyglucose positron emission tomography pattern of pulmonary lymphangitic carcinomatosis. *J Comput Assist Tomogr.* 2005;29:346–349.
9. Cohen JF, Korevaar DA, Altman DG, et al. STARD 2015 guidelines for reporting diagnostic accuracy studies: explanation and elaboration. *BMJ Open.* 2016;6:e012799.
10. Gurda GT, Zhang L, Wang Y, et al. Utility of five commonly used immunohistochemical markers TTF-1, Napsin A, CK7, CK5/6 and P63 in primary and metastatic adenocarcinoma and squamous cell carcinoma of the lung: a retrospective study of 246 fine needle aspiration cases. *Clin Transl Med.* 2015;4:16.
11. Lin LI. A concordance correlation coefficient to evaluate reproducibility. *Biometrics.* 1989;45:255–268.
12. Liu X. Classification accuracy and cut point selection. *Stat Med.* 2012;31:2676–2686.
13. DeLong ER, DeLong DM, Clarke-Pearson DL. Comparing the areas under two or more correlated receiver operating characteristic curves: a nonparametric approach. *Biometrics.* 1988;44:837–845.
14. Detterbeck FC, Boffa DJ, Kim AW, Tanoue LT. The eighth edition lung cancer stage classification. *Chest.* 2017;151:193–203.
15. Soares FA, Pinto AP, Landell GA, de Oliveira JA. Pulmonary tumor embolism to arterial vessels and carcinomatous lymphangitis: a comparative clinicopathological study. *Arch Pathol Lab Med.* 1993;117:827–831.
16. Lindqvist C, Lepantalo M, Jungell P. Lymphangitis carcinomatosa of the lungs: an unusual complication of oral cancer. *Br J Oral Maxillofac Surg.* 1988;26:228–231.
17. Sakuma M, Fukui S, Nakamura M, et al. Cancer and pulmonary embolism: thrombotic embolism, tumor embolism, and tumor invasion into a large vein. *Circ J.* 2006;70:744–749.
18. Roberts KE, Hamele-Bena D, Saqi A, Stein CA, Cole RP. Pulmonary tumor embolism: a review of the literature. *Am J Med.* 2003;115:228–232.
19. King MB, Harmon KR. Unusual forms of pulmonary embolism. *Clin Chest Med.* 1994;15:561–580.
20. Bassiri AG, Haghighi B, Doyle RL, Berry GJ, Rizk NW. Pulmonary tumor embolism. *Am J Respir Crit Care Med.* 1997;155:2089–2095.
21. Moubax K, Wuyts W, Vandecaveye V, Prenen H. Pulmonary lymphangitic carcinomatosis as a primary manifestation of gastric carcinoma in a young adult: a case report and review of the literature. *BMC Res Notes.* 2012;5:638.
22. Gonzalez-Vitale JC, Garcia-Bunuel R. Pulmonary tumor emboli and cor pulmonale in primary carcinoma of the lung. *Cancer.* 1976;38:2105–2110.
23. Chan CK, Hutcheon MA, Hyland RH, Smith GJ, Patterson BJ, Matthay RA. Pulmonary tumor embolism: a critical review of clinical, imaging, and hemodynamic features. *J Thorac Imaging.* 1987;2:4–14.
24. Shepard JA, Moore EH, Templeton PA, McLoud TC. Pulmonary intravascular tumor emboli: dilated and beaded peripheral pulmonary arteries at CT. *Radiology.* 1993;187:797–801.
25. Munk PL, Muller NL, Miller RR, Ostrow DN. Pulmonary lymphangitic carcinomatosis: CT and pathologic findings. *Radiology.* 1988;166:705–709.
26. Johkoh T, Ikezoe J, Tomiyama N, et al. CT findings in lymphangitic carcinomatosis of the lung: correlation with histologic findings and pulmonary function tests. *AJR.* 1992;158:1217–1222.
27. Hou S, Lin X, Wang S, et al. Combination of positron emission tomography/computed tomography and chest thin-layer high-resolution computed tomography for evaluation of pulmonary nodules: correlation with imaging features, maximum standardized uptake value, and pathology. *Medicine (Baltimore).* 2018;97:e11640.